Study of the degradation of Bezaktiv Brilliant Blue by the Fenton process using a prepared ferromagnetic activated carbon from rubber seed hull as heterogeneous catalyst

Sandrale Grace Mokue Mafo[a], Donald Raoul Tchuifon Tchuifon[a,b],*, Christian Sadeu Ngakou[a], Cyrille Ghislain Fotsop[c], Paul Alain Nanssou Kouteu[b,d],*, Giscard Doungmo[e], George Nche Ndifor-Angwafor[a],*, Solomon Gabche Anagho[a]

[a]*Department of Chemistry, Research Unit of Noxious Chemistry and Environmental Engineering, Faculty of Science, University of Dschang, P.O. Box: 67, Dschang, Cameroon, emails: sandralemafo@gmail.com (S.G.M. Mafo), cs_ngakou@yahoo.com (C.S. Ngakou), nchegeorged4@yahoo.com (G.N. Ndifor-Angwafor), sg_anagho@yahoo.com (S.G. Anagho)*
[b]*Department of Process Engineering, Laboratory of Energy, Materials, Modeling and Method, National Higher Polytechnic School of Douala, University of Douala, P.O. Box: 2701, Douala, Cameroon, email: tchuifondonald@yahoo.fr (D.R.T. Tchuifon)*
[c]*Institute of Chemistry, Faculty of Process and Systems Engineering, Universität Platz 2, 39106 Magdeburg, Germany, email: fotsopcyril@yahoo.fr (C.G. Fotsop)*
[d]*Process Engineering Laboratory, Ucac-Icam Institute, P.O. Box: 5504 Douala, Cameroon, email: kpaulous@yahoo.fr (P.A.N. Kouteu)*
[e]*Institut für Anorganische Chemie, Christian-Albrechts-Universität zu Kiel, Max-Eyth-Str. 2, 24118 Kiel, Germany, email: giscar99@yahoo.fr (G. Doungmo)*

ABSTRACT

A ferromagnetic activated carbon, CA-HP@FeII was used as a heterogeneous catalyst in the Fenton oxidation process for the removal of Bezaktiv Brilliant Blue dye from contaminated water. It was prepared by optimizing the activation of rubber seed hull with phosphoric acid, modified with iron(II) sulfate. The ferromagnetic activated carbon was characterized by Fourier-transform infrared spectroscopy, X-ray diffraction, scanning electron microscopy/energy-dispersive X-ray spectroscopy, Brunauer–Emmett–Teller and pore-size distribution. The characterized activated carbon was used to study the degradation of the Bezaktiv Brilliant Blue dye by varying several parameters, namely the pH of the solution, the concentration of H_2O_2 solution, the mass of the catalyst, and the concentration of the pollutant. The results of the characterization showed that ferromagnetite was deposited on the activated carbon during the modification process and the obtained ferromagnetic activated carbon have a cubic spinel structure and a specific area of 110.53 $m^2 \cdot g^{-1}$. The elimination of the dye was favorable at the acid pH of 3. The removal of the pollutant was favorable when the concentration of H_2O_2, the mass of the catalyst and the concentration of the pollutant were increased. The final elimination percentage was greater than 75%, whatever the condition and the parameter varied. The second-order kinetic model better described the degradation of Bezaktiv Brilliant Blue pollutant on CA-HP@FeII. An analysis of the ferromagnetic material after degradation showed that it had undergone very little changes, and hence could be reused several times. The change in the percentage of carbon from 46.54% to 54.86% in the ferromagnetic activated after degradation can be attributed to the mineralization of the carbon atoms of Bezaktiv Brilliant Blue.

Keywords: Ferromagnetic activated carbon; Fenton degradation process; Bezaktiv Brilliant Blue

* Corresponding authors.

1. Introduction

One of the most used adsorbents in industrial processes is activated carbon. It generally has high surface area with microporous and heterogeneous structures. The production of activated carbon with the highest adsorption properties has not been extensively investigated [1]. Nowadays, the main objective for researchers is to produce activated carbons with high adsorption properties using inexpensive and effective alternatives to those used for commercial ones [2,3]. Lignocellulosic materials are continually gaining enormous attention as raw materials in the production of adsorbents [4–6].

Generally, the mechanism of activating lignocellulosic materials compromises three different stages: intense depolymerisation of the activating carbon precursor at temperatures between 0°C and 300°C; devolatilization and formation of the inner porosity between 300°C and 700°C; and dehydrogenation of the fixed carbon structure above 700°C [7]. During the synthesis of activated carbons, the most relevant parameters that control the final properties are the activating temperature, the impregnation ratio of the activating agent, and the calcination time [7].

Researchers have been using the Methodology of Experimental Design to investigate the effect of the above parameters on the production of activated carbons [8,9]. This method is based on the deduction of equations or mathematical models of the production process using the relevant parameters, and then validating the models by statistical techniques. In recent years, some authors have applied these optimization methods to the production of activated carbons [1,8–10]. The resulting activated carbons due to their structure and surface area have been proposed as suitable options for the removal of organic contaminants from aqueous solutions. Unfortunately, using activated carbons on large scales have had some limitations because of difficulties associated with filtration, dispersion, turbidity and high cost of its production [11].

Recently, magnetic separation methods have been widely used due to their low cost, simplicity and high speed of separation with high efficiency. Many adsorbents are magnetized [12], and the presence of magnetic iron oxide leads to chemical stability, low toxicity, and excellent recyclability of adsorbent. These have been some of the reasons for their wide use in removing toxic ions and organic contaminants from water and wastewater [13]. Conventional treatments such as adsorption onto activated carbon, membrane processes, coagulation–flocculation, chemical oxidations, have the disadvantage of transferring pollutants from an aqueous phase to a new phase, leading in the most part to the formation of concentrated sludge, thus creating a problem of secondary waste disposal, as well as giving rise to very expensive regeneration of the adsorbent materials.

Among all the possible treatment techniques for contaminated aqueous effluents, advanced oxidation processes (AOPs) using the Fenton process appear to be the processes of choice. They lead to the total degradation of the pollutant as well as a reduction in the overall toxicity of the effluent. AOPs are essentially based on the production of active and not very specific species such as hydroxyl radicals, which on interacting with the toxic pollutant degrades them to nontoxic species that can be freely disposed of [14]. In Fenton processes, the catalyst supported on the solid matrices have certain advantages. For example, because it is highly conductive, ferromagnetic activated carbons allow the pollutants to concentrate around the catalyst and decompose effectively [15]. Studies also reveal that activated carbon is a good support for iron species and the supported iron can be used as a heterogeneous Fenton catalyst [16]. Due to the need to search for optimal conditions to produce activated carbon with the desired properties, the response surface methodology was chosen to do the modelling of the production process. According to Aydar [17] many other works found in the literature, the response surface methodology investigates an appropriate approximate relationship between input and output variables and identify the optimal operating conditions for the system under study.

Therefore, it is hypothesized that optimisation of the process of preparing activated carbon using response surface methodology and its modification to ferromagnetic activated carbon would give activated carbon with better characteristics for the greater adsorption and degradation of contaminants relative to non-magnetic activated carbons [18]. The specific objectives of this study are: (a) to prepare activated carbon using the methodology of experimental design from rubber seed hulls, (b) to modify the activated carbon to ferromagnetic activated carbon (c) to characterize the prepared and magnetic activated carbons by physico-chemical techniques, and (d) to use the ferromagnetic activated carbon to study the Fenton degradation of Bezaktiv Brilliant Blue in aqueous solution.

2. Materials and methods

2.1. Material and reagents

All chemicals used in this work are analytical grade. Bezaktiv Brilliant Blue dye (its characteristics are given in Table 1) was obtained from CICAM, a textile industry located in Douala, Cameroon. H_2O_2 (50% w/w) and $FeSO_4 \cdot 7H_2O$ (Fisher Scientific), H_3PO_4, H_2SO_4 and NaOH (Sigma-Aldrich) were used as received. Bezaktiv Brilliant Blue dye was selected because of its common use in the CICAM textile industry to dye fabric and its negative impact on the environment.

Table 1
Characteristic of Bezaktiv Brilliant Blue

Parameter	Amount
Chemical formula	$C_{12}H_{16}O_{11}N_2S_3Na_2$
Molecular weight	626.5 g/mol
m/z	443
Molecular structure	
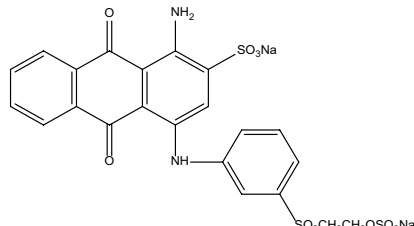
2.2. Preparation of activated carbon

The rubber seed shells used to prepare activated carbon were harvested from the rubber plantations of SOCAPALM (Cameroonian Society of Palm Groves). The collected rubber seed shells were washed, dried in an oven set at 105°C and then crushed to obtain particles of sizes between 1 and 2 mm.

The centered composite plan was used to optimize the preparation of the activated carbon, in order to determine the factors needed to obtain the most microporous activated carbon. The factors investigated in this study are the concentration of activating agents (X_1), the calcination temperature (X_2) and the residence time (X_3). The mathematical model used to evaluate the interactions of the different factors on the response is of the form:

$$Y = \alpha_0 + \sum_{i=1}^{n} \alpha_i X_i + \sum_{i=1}^{n} \alpha_{ii} X_i^2 + \sum_{i=1}^{n} \sum_{j=1}^{n} \alpha_{ij} X_i X_j \qquad (1)$$

where Y is the predicted response, X_i and X_j are the coded values of the factors, α_0, α_i, α_{ii} and α_{ij} are the constant, linear coefficients, quadratic coefficients and interaction coefficients, respectively. The experimental data were analyzed using Statgraphics Plus 5 software to run the regression analysis to determine the constant and the coefficients of the mathematical model fit the equations developed and also to evaluate the statistical significance of the equations obtained.

The following protocol was used for the preparation of activated carbon impregnated with phosphoric acid as activating agent (CA-HP). 20 g of rubber seed hulls were mixed with 50 mL solutions of phosphoric acid of different concentrations (0.5–2.0 mol/L) for 24 h and dried at 105°C in an oven for 12 h. After impregnation, the mixtures were carbonized between 400°C–600°C in the furnace Select-Horn. The activated carbons obtained were washed, dried and crushed.

2.3. Modification of the activated carbon

Ferromagnetic activated carbons were prepared as follows: 5 g of activated carbons (CA-HP) were introduced into 250 mL of an aqueous solution containing 5 g of NaOH and 10 g of $FeSO_4 \cdot 7H_2O$. The whole combination was stirred at a temperature of 70°C for 1 h, filtered and the residue dried in an oven at 110°C for 24 h.

2.4. Adsorption of iodine: adsorption capacity of the activated carbons

Iodine was considered as probe molecule for determining the adsorption capacity of the adsorbents for solutes of molecular sizes less than 10 Å. The iodine number was estimated by shaking a mixture of 0.1 g of activated carbon with 0.02 N iodine solution for 3 h, and then titrating the resulting solution against 0.005 M $Na_2S_2O_3$ solution [19].

2.5. Characterization of activated carbon and magnetic activated carbon

The produced activated carbon and ferromagnetic activated carbon were characterized by using Fourier-transform infrared spectroscopy (FTIR), X-ray diffraction (XRD), energy-dispersive X-ray spectroscopy (EDX), specific surface by the Brunauer–Emmett–Teller (BET) method and pore-size distribution.

2.5.1. Fourier-transform infrared spectroscopy

FTIR spectra were obtained on a Genesis FTIR Spectrometer (Bruker Optik GmbH, Rudolf-Plank-Str. 27, 76275 Ettlingen, Germany) (ATI Mattson) equipped with a DTGS (deuterated triglycine sulfate) detector in the transmission mode from 400 to 4,000 cm^{-1} after 20 scans.

2.5.2. X-ray diffraction

Ex-situ XRD data was collected on a STOE STADI P powder diffractometer (Stoe & CIE GmbH, Darmstadt, Germany) with Cu-Kα1 radiation (λ = 1.54056 Å; Ge monochromator; flat samples) in transmission geometry with a DECTRIS® MYTHEN 1K detector (DECTRIS, Baden-Daettwil, Switzerland).

2.5.3. Scanning electron microscopy/energy-dispersive X-ray spectroscopy

Field-emission scanning electron microscopy coupled with energy-dispersive X-ray microanalysis (FE-SEM/EDX) were performed on the activated carbon and the ferromagnetic activated carbons using a Magellan 400L Scanning Electron Microscope.

2.5.4. Specific surface area by the BET method

The specific surface area of a sample of material represents the accessible surface per unit of mass. It corresponds to the sum of the internal surface and the external surface of the particles contained in the sample. Thus, it depends on the shape of the particles but especially on their dimensions. The determination of the specific surface is based on the adsorption of the nitrogen molecule at 77 K. During the analysis stage, the activated carbon was placed in a sample holder bulb which was then immersed in a vase containing liquid nitrogen (at 77.13 K). A stream of nitrogen under different pressures then circulated inside the bulb and was adsorbed on the activated carbon. Sorption experiments were recorded using a Bel Japan Inc. BELSORP MAX Apparatus. Prior to the experiments, all samples were thermally treated under reduced pressure (10 Pa) at 150°C for 16 h. The nitrogen sorption isotherms were measured at 77 K, and the specific surface areas were determined by the BET method. The Barrett–Joyner–Halenda (BJH) method was used to obtain pore-size distribution from the desorption segment of the nitrogen adsorption/desorption isotherms.

2.6. Fenton oxidation experiments using synthesized catalyst

The Fenton oxidation experiments were carried out at room temperature in an Erlenmeyer flask with a volume of 1 L as a reactor. A stock solution of 1,000 mg/L of dye was serially diluted to obtain the daughter solutions to be used. The Fenton oxidation was carried out by varying the pH from

2 to 4, the mass of activated carbon from 0.16–1 g/L, the concentration of H_2O_2 from 4–17 mol/L, and the dye or pollutant concentration from 50–150 mg/L. The residual concentration of the dye in the reaction mixture at different reaction times were determined by measuring the absorption intensity at $\lambda_{max} = 610$ nm and a calibration curve. The degradation efficiency of Bezaktiv Brilliant Blue is defined as follows:

$$\text{Degradation efficiency}\,\left(\%\right) = 100\left(1\frac{C_t}{C_o}\right) \tag{2}$$

where the C_o is the initial concentration of Bezaktiv Brilliant Blue and C_t is the concentration of Bezaktiv Brilliant Blue at reaction time t (min).

3. Results and discussion

3.1. Biomass analysis

After carrying out the experiments to determine the dry matter and the organic matter of the rubber seed shells, the results in Table 2 were obtained.

The dry matter was obtained as 97.82% of the biomass used, and organic matter was 98.74% of dry matter. These values are much higher than 50%, meaning that this biomass could be subject to an additional test to determine the composition of the different types of organic fibers present in it. According to Table 1 the quantities of cellulose, hemicellulose and lignin in percentages of dry matter, respectively 29.64%, 21.51% and 41.07%. These high values show that this biomass is rich in carbon and poor in inorganic elements. Also, the small value of the observed ash content shows that this biomass can be used for the production of activated carbon [8].

3.2. Preparation of activated carbon

The runs from the experimental design and the respective responses are presented in Table 3, while Tables 4 and

Table 2
Percentages of dry matter, organic matter, ash and quantity of lignin, cellulose and hemicellulose in Hevea fruit shells

Constituents	(% MS)
DM	97.82
OM	98.74
Ash	1.26
GP	2.89
FAT	1.36
NDF	92.22
ADF	70.71
ADL	41.07
C	29.64
HMC	21.51

DM = dry matter; GP = gross protein; OM = organic matter; NDF = neutral detergent fiber; ADF = acid detergent fiber; ADL = lignin detergent acid; C = cellulose; HMC = hemicellulose.

5 show the analysis of variance (ANOVA) analysis and the combinations of factors which give highest response values. Eq. (2) is the mathematical model of the parameters of composite activated carbon that result from the experimental runs.

A close observation of the results affirms that the yields of activated carbons vary from 33.68% to 56.12% by mass of the biomass. The yields obtained depend on the calcination temperature and also on the duration of the calcination in the furnace. The yield decreases with increasing calcination time and with increasing temperature. The mass loss can then be explained by the departure of oxygen and hydrogen molecules in the forms of the gases H_2O, CO, CO_2, CH_4, and aldehydes [20,21]. As for the iodine index, values between 234.13 and 529.17 mg/g have been observed. Generally, the higher the iodine number, the greater the adsorption capacity, since it indicates the degree of porosity of the material. The two factors that determine the high values of iodine number are the activation temperature and the duration of the calcination, because these factors play a major role in the development of the pores of the activated carbon. For example, the high iodine number of 529.17 mg/g was obtained at the high temperature of 600°C for and the high calcination time of 120 min.

The ANOVA of the optimization process shows that concentration of the activating agent and the temperature of calcination have *P*-values less than 0.05. These values indicate that the two factors increase the iodine number of the activated carbon [22]. This can be explained by the fact that, phosphoric acid catalyses the reaction of acid dehydration, promotes depolymerisation reactions of lignocellulosic matter and facilities the loss of hydrogen, thereby favouring the enrichment in carbon. They can also favour the formation of aromatic rings of the activated carbon [1]. The results of the ANOVA mentioned in Table 3, also indicate that the linear effect and the quadratic effect of temperature significantly influence the iodine number, with the former influencing positively and the later influencing negatively. This means that for low temperature values investigated (300°C–550°C), temperature contributes to the development of microporosity, while at high temperature values (>600°C) there is a decrease in the microporosity (Fig. 1). These results can be explained by saying that initially, there is an increase in the devolatilization and swelling of the biomass with temperature rise. This is followed by a subsequent collapse of the pore structure with further increase in the temperature [23]. These results are similar to those of Tay et al. [24] who showed that the volume of the micropores of the activated carbon produced from soybean oil cake increased until the carbonization temperature reaches 650°C and at a higher temperature, the volume of micropores decreased. The authors concluded that a temperature higher than 650°C led to the passage from micropores to mesopores.

On the other hand, the high *P*-value in the case of time may be due to the fact that as calcination time increases, the amount of volatile matter increases, thereby reducing the amount of micropores in the activated carbon. The combination between the concentration and temperature gives synergetic effect while the combination of one of them with time gives antagonist effect. In the mathematical equation a positive sign in front of the coefficients indicates synergistic

Table 3
Experimental design and the corresponding experimental responses

Experiment	X_1	X_2	X_3	Y_1: Iodine number (mg/g)		Y_2: Yield	
				Observed value	Predicted value	Observed value	Predicted value
1	1.25	600.00	82.50	382.60	374.14	39.30	42.92
2	1.25	500.00	82.50	350.24	379.04	51.70	49.05
3	1.25	400.00	82.50	234.13	252.70	61.80	56.12
4	1.25	500.00	82.50	394.02	379.04	44.08	49.05
5	2.00	400.00	45.00	331.21	321.19	53.24	54.42
6	0.50	400.00	120.00	302.65	292.44	45.70	46.84
7	2.00	500.00	82.50	340.73	357.39	52.50	50.26
8	0.50	600.00	45.00	493.00	495.54	37.12	35.38
9	2.00	400.00	120.00	317.88	312.81	49.70	51.96
10	0.50	600.00	120.00	529.17	536.66	34.35	33.68
11	1.25	500.00	45.00	403.54	396.60	45.94	46.02
12	0.50	500.00	82.50	441.61	435.05	44.62	44.80
13	0.50	400.00	45.00	249.36	256.10	47.81	48.91
14	2.00	600.00	45.00	312.17	319.85	41.80	41.18
15	2.00	600.00	120.00	325.50	316.24	39.67	39.08
16	1.25	500.00	82.50	413.06	379.04	47.25	49.04
17	1.25	500.00	120.00	395.93	412.97	46.07	43.93

X_1: concentration (mol/L); X_2: activation temperature (°C); X_3: activation time (min).

Table 4
Analysis of variance for iodine number

Source	Iodine number (mg/g)					Yield %				
	Sum of squares	df	Mean square	F-ratio	P-value	Sum of squares	df	Mean square	F-ratio	P-value
X_1: concentration	15,077.70	1	15,077.70	28.00	***0.0011***	74.58	1	74.58	5.06	0.0592
X_2: temperature	36,870.40	1	36,870.40	68.46	***0.0001***	435.73	1	435.73	29.58	***0.0010***
X_3: time	669.94	1	669.94	1.24	0.3015	10.86	1	10.85	0.74	0.4190
X_1X_1	791.33	1	791.33	1.47	0.2648	6.17	1	6.17	0.42	0.5382
X_1X_2	28,989.90	1	28,989.90	53.83	***0.0002***	0.04	1	0.04	0.00	0.9596
X_1X_3	1,000.39	1	1,000.39	1.86	0.2151	0.08	1	0.08	0.01	0.9440
X_2X_2	11,536.50	1	11,536.50	21.42	***0.0024***	0.60	1	0.60	0.04	0.8460
X_2X_3	11.38	1	11.38	0.02	0.8885	0.07	1	0.07	0.00	0.9469
X_3X_3	1,776.63	1	1,776.63	3.30	0.1122	44.44	1	44.44	3.02	0.1260
Total error	3,769.81	7	538.54			103.12	7	14.73		
Total (Corr.)	98,007.70	16				718.17	16			

R-squared = 0.9615		R-adjusted = 0.9121		R-squared = 0.8564		R-adjusted = 0.6717

effects, whereas a negative sign indicates antagonistic effects. The R-squared statistics obtained indicates that the model as fitted explains 96.15% of the variability in iodine number. The adjusted R-squared statistics, which is more suitable for comparing models with different numbers of independent variables, is 91.21% and therefore indicates a high significance for the model [25,26]. The standard error of the estimate shows the standard deviation of the residuals to be 7.42. The low values of the coefficient of determination (R^2) and the adjusted coefficient of determination (R^2-adj.) are an indication that the mathematical model chosen is not appropriate to describe the results concerning the yield.

3.3. Mathematical modeling of responses

All responses were used to develop quadratic model regression equations with second-order interaction that correlates each response with the three coded variables. The

polynomial model equation in terms of the coded factors obtained after optimization is given by iodine number (Y_1) and yield (Y_2) as responses:

$$\begin{aligned}
\text{Iodine number}\left(Y_1\right) = &-1{,}875.49 + 305.963X_1 \\
&+ 8.14618X_2 - 2.46517X_3 + 30.5527X_1X_1 \\
&- 0.802633X_1X_2 - 0.3976X_1X_3 - 0.00656191X_2X_2 \\
&+ 0.000318X_2X_3 + 0.0183118X_3X_3
\end{aligned} \tag{3}$$

$$\begin{aligned}
\text{Yield}\left(Y_2\right) = &\ 68.9424 + 10.2006X_1 - 0.116506X_2 \\
&+ 0.441946X_3 - 2.69784X_1X_1 + 0.00095X_1X_2 \\
&- 0.00351111X_1X_3 + 0.0000472465X_2X_2 \\
&+ 0.000025X_2X_3 - 0.00289603X_3X_3
\end{aligned} \tag{4}$$

Fig. 1 gives the curves of the three-dimensional response surfaces which are the graphical representations of the regression equation for the optimization of the three reaction variables, namely the concentration (X_1), the temperature (X_2), and the time of calcination (X_3).

Regarding Fig. 1, it can be seen that the iodine number increases with an increase in temperature. This is explained by the fact that when the calcination temperature increases, the volatile materials evaporated increase. Consequently, some pores are dilated while more pores are created thereby increasing the adsorption sites [27]. In addition, an increase in the concentration of activating agents leads to an increase in the iodine index. Amola et al. also reported similar results [28]. For the activated carbon resulting from our work, the results of Table 3 indicate that the X_1X_2, that is, the concentration-temperature interaction is significant with a probability $P = 0.0002$ for the iodine number. It can also be seen from the same table that the concentration and temperature interaction with P of 0.0011 and 0.0001 have a significant influence on the iodine number.
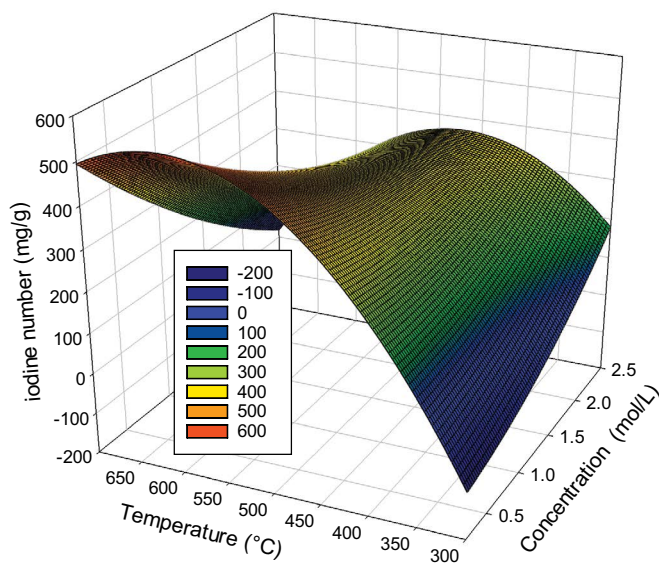
3.4. Characterizations

3.4.1. FTIR spectrums

The FTIR spectroscopy was used to determine the various functional groups present in the raw material and both activated carbons. The spectra obtained are shown in Fig. 2.

Rubber seed shells exhibit hydroxyl functional groups, including hydrogen bonding (3,600–3,200 cm^{-1}), which is much less prevalent in both activated carbons. Hydrogen bonds are reduced in the presence of phosphoric acid, which shows that phosphoric acid acts as a dehydrating agent by reacting with the raw material. The intense band at approximately 2,900 cm^{-1} is assigned to C–H stretching, which is reduced in the activated carbons indicating that the activation process reduces significantly the hydrogen
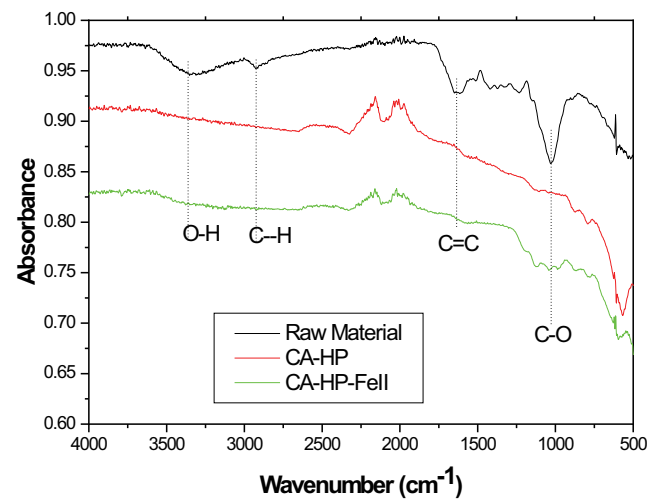

Fig. 2. Fourier-transform infrared spectra: raw rubber seed shells, activated carbon (CA-HP) and magnetic activated carbon (CA-HP@FeII).
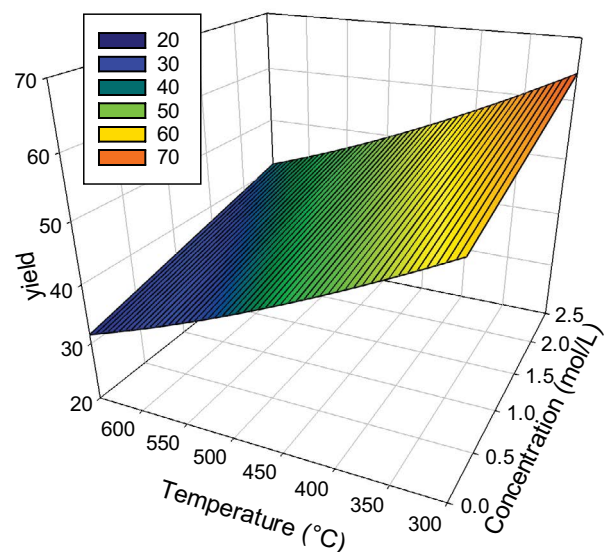

Fig. 1. Contours of the 3-dimensional response surface in the case of iodine number and carbon yield.

amount [29]. The stretching absorption band between 1,550–1,680 cm^{-1} can be attributed to –C=C vibration while the one at 1,300–1,050 cm^{-1} can be attributed to –C–O vibration in carboxylic acids and –C–O vibration in lactones. The last stretching absorption band between 900–600 cm^{-1} can be attributed to vibration of aromatic polynuclear systems [19]. Furthermore, there is clearly a decrease in the intensity of the bands between 1,700–1,500 cm^{-1}. This may indicate that iron is being bound to these functional groups. It may also be an oxygen-metal bond, since a band around 770 cm^{-1} is present [30]. This shows that during activation, there was a breakdown of C–H bonds to form new C–R bonds. The peaks at 1,650 and 1,031 cm^{-1} assigned to the aromatic rings and alcohols, respectively disappeared likewise in the activated carbons. However, new peaks recorded in the region 1,150–750 cm^{-1}, were observed for carbons activated with phosphoric acid and they are attributed to the presence of phosphorus-containing groups such as P=O bonds in a phosphoric ester, O–C in P–O–C or P=OOH [31].

3.4.2. XRD patterns

XRD was used to determine the crystallinity of the raw material and both activated carbons. The patterns obtained are shown in Fig. 3.

In the case of the raw material one peak is observed at $2\theta = 26°$. This can be attributed to the different planar crystal structure of carbon [32]. The absence of peaks on the pattern of the activated carbon indicates amorphous carbon with a chaotic layer due to the breaking of ester bonds between lignin and other components during H_3PO_4 pretreatment and carbonization of the rubber seed husks. This can be attributed to the activation temperature which is less than 600°C; a temperature at with crystallinity is well developed [7]. Furthermore, the pattern from the magnetic activated carbon shows many peaks. The ones around $2\theta = 30°$ and $2\theta = 43°$ can also be attributed to the planar crystal structure of activated carbon [32]. The diffractogram clearly reveals the presence of several peaks, thereby indicating the existence of different crystalline phases containing iron within the carbon
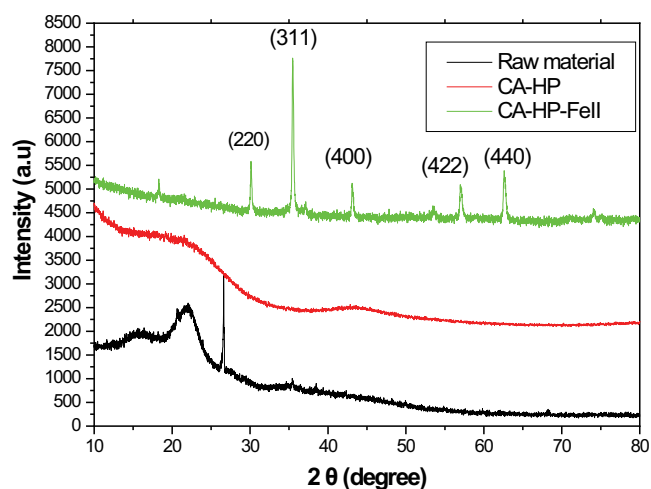
matrix of the modified activated carbon. The presence of crystalline phases of iron confirms the insertion of iron ions in the carbon. These crystalline phases consist essentially of magnetite (Fe_3O_4) and maghemite (γ-Fe_2O_3) at $2\theta = 35°$. Only magnetite (Fe_3O_4) has a ferromagnetic character, the other phase is paramagnetic. The peak of activated carbon-Fe_3O_4 composite confirmed the existence of Fe_3O_4 peak at 2θ value of 30°, 35°, 43°, 54° and 65° which indicate cubic spinel structure of peaks indexed as (220), (311), (400), (422) and (440).

3.4.3. Scanning electron microscopy/EDX analysis

Scanning electron microscopy coupled with energy-dispersive X-ray microanalysis (SEM/EDX) with its X-ray dispersion spectroscopy imaging in the chemical analysis modes contribute to the morphological characterization and chemical analysis of samples. Fig. 4A presents the results of the EDX while that of 4B presents the SEM result of the iron(II) modified activated carbon.

It can be seen from the chromatogram in Fig. 4A that iron is actually introduced into the material. The presence of sulfur as well as sodium in this material can be attributed to the reagents NaOH and $FeSO_4$ used. The elements

Fig. 3. X-ray diffraction patterns of raw material and both activated carbons.
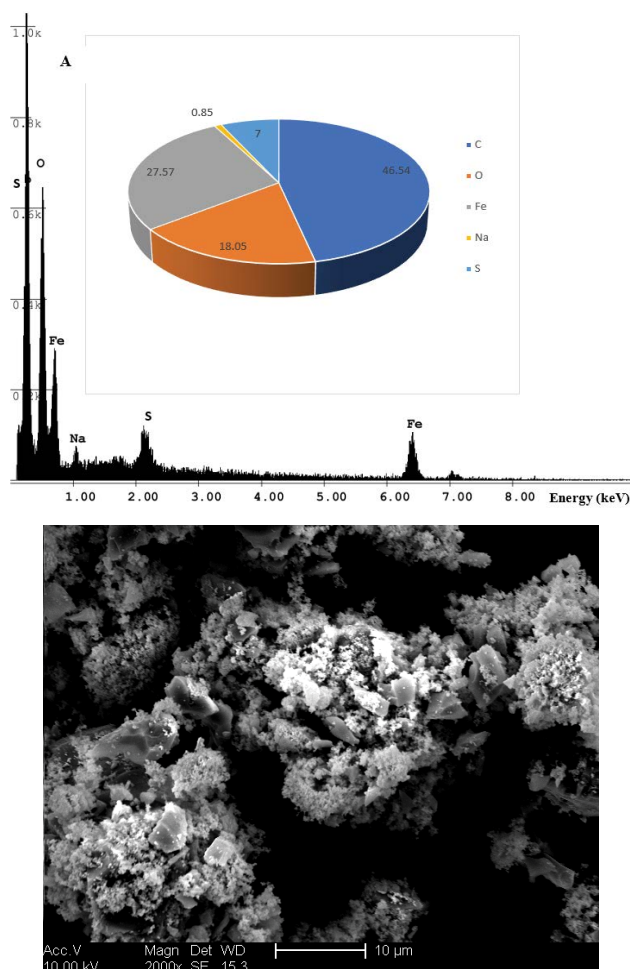

Fig. 4. Energy-dispersive X-ray spectroscopy analysis (A) and scanning electron microscopy image (B) of CA-HP@FeII.

encountered in the material are C (46.54%), Fe (27.57%), O (18.05%), S (7%) and Na (0.85%). The absence of hydrogen is justified by the fact that this technique only takes into account atoms with atomic numbers greater than or equal to 5. The morphology of the material does not present pores because the latter have been modified by the reaction of NaOH and $FeSO_4$ to obtain the new material that has a magnetic character.

3.4.4. BET/Barrett–Joyner–Halenda analysis

Table 6 and Fig. 5 below show the results obtained during the BET/Barrett–Joyner–Halenda (BHJ) analysis of CA-HP@FeII.

The adsorption hysteresis obtained during the BET analysis shows the formation of a monolayer due to the adsorption of nitrogen by the micropores present in the ferromagnetic activated carbon followed by multilayer adsorption on the external surface [33]. The BET analysis revealed that the specific surface area of CA-HP@FeII is 110.53 $m^2 \cdot g^{-1}$. This low surface area is in agreement with the SEM analysis which presented a material surface that did not have

Table 5
Factors which give highest iodine number

Concentration (mol/L)	0.5
Activation temperature (°C)	593.07
Activation time (min)	120.0
Iodine number (mg/g)	
- Predicted	536.98
- Observed	544.40
Yield %	
- Predicted	57.38
- Observed	34.06

Table 6
BET specific surface area, total volume and average pore diameter of CA-HP@FeII

	BET	
V_m	25.40	$(cm^3 \ (STP) \ g^{-1})$
$a_{s,BET}$	110.53	$(m^2 \cdot g^{-1})$
C	775.77	
Total pore volume		
$(p/p_0 = 0.500)$	0.05	$(cm^3 \cdot g^{-1})$
Mean pore diameter	1.87	(nm)
	BJH	
Plot data	Desorption branch	
Standard t curve data	Harkins–Jura-BEL·t	
V_p	0.09	$(cm^3 \cdot g^{-1})$
$d_{p,peak}$ (Area V_p)	2.00	(nm)
S_p	75.67	$(m^2 \cdot g^{-1})$
Average diameter of pores	5.02	(nm)
Middle diameter of pores	17.32	(nm)

pores. This result therefore confirms that the iron oxide Fe_3O_4 (magnetite) has occupied the active sites of the material. The analysis of the pore size by the BHJ method highlights the microporous character of the ferromagnetic activated carbon obtained. Similar results were obtained by Kpinsoton [34] during his work on the development of catalysts based on activated carbons and laterites for the degradation of methylene blue by heterogeneous Fenton process.

3.5. Degradation of Bezaktiv Brilliant Blue dye in aqueous solution

3.5.1. Influence of pH on the degradation process

The effect of pH on the degradation of Bezaktiv Brilliant Blue by the Fenton process was studied at different pH values; using Bezaktiv Brilliant Blue of initial concentration 100 mg/L. The results obtained are shown in Fig. 6.

The results presented in Fig. 6 show that the catalytic efficiency increases with decreasing pH. The maximum degradation of Bezaktiv Brilliant Blue is observed at pH = 2 after 240 min with a degradation rate of 96.46%. The effect of the initial pH of the solution on the degradation is very important because it influences the surface electric charge of the catalyst. Indeed, in acid medium, a strong adsorption of the dye on the surface of the oxide is observed. This is probably due to the electrostatic attraction of the positive charge of the
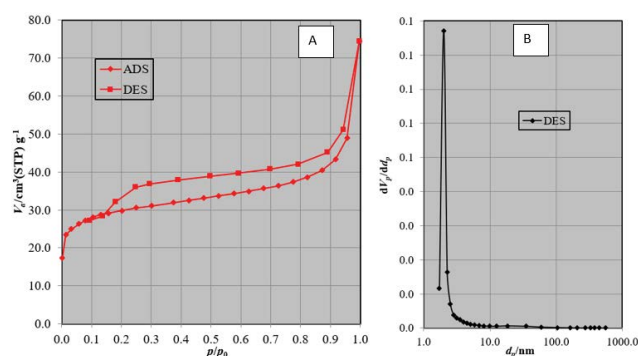

Fig. 5. Adsorption hysteresis (A) and pore-size distribution (B) of CA-HP@FeII material.
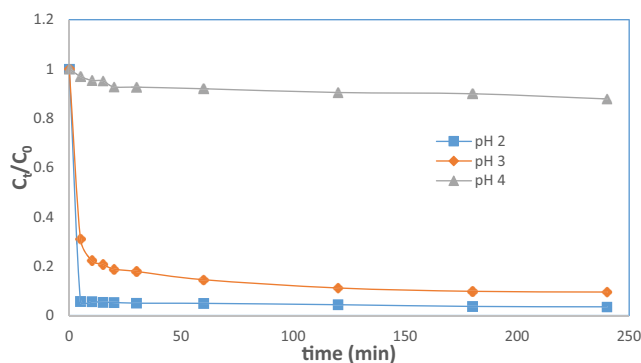

Fig. 6. Influence of pH on the Fenton degradation of Bezaktiv Brilliant Blue. Operating conditions: v = 150 mL, m = 50 mg, C_0 = 100 mg/L and $[H_2O_2]$ = 17 mol/L.

ferromagnetic activated carbon and the negative charge of the dye. This can be explained by the fact that Fe^{2+} is more stable at pH = 2 and formation of complexes start at pH = 4 [35,36]. The equation of the formation of complexes is:

$$Fe^{2+} + H_2O \rightarrow \left[FeOH \right]^+ + H^+ \tag{5}$$

However, several works on the degradation by the Fenton process have shown that pH values between 2 and 3 are optimal for the elimination of organic pollutants, since at pH greater than or equal to 4, the degradation decreases due to the precipitation of Fe^{3+} ions in the form of $Fe(OH)_3$. In addition, the oxidation potential of hydroxyl radicals decreases with increasing pH, which could be due to the dissociation and self-decomposition of H_2O_2 [37]. Therefore, the presence of ferromagnetic activated carbon in the medium ensures that there is continuous supply of Fe^{2+}, giving rice to a significant percentage of degradation at a pH of 3.

3.5.2. Influence of the mass of ferromagnetic activated carbon

To highlight the influence of mass on the degradation of Bezaktiv Brilliant Blue, experiments were run for masses of ferromagnetic activated carbon varying from 0.16 to 1 g/L, but keeping the concentration of Bezaktiv Brilliant Blue constant. The results obtained are shown in Fig. 7.

The results in Fig. 7 show that an increase in the mass of the ferromagnetic activated carbon, CA-HP@FeII leads to an increase in the amount of Bezaktiv Brilliant Blue degraded. This is explained by the fact that the Fe^{2+} acts as a catalyst that initiates the decomposition of H_2O_2 to generate the OH radical. However, at masses greater than 50 mg, the percentage removal of Bezaktiv Brilliant Blue begins to decrease sharply after more than 120 min of contact time. This noticeable decrease in the rate of degradation can be attributed to the fact that the initial rate of formation of hydroxyl radicals from the decomposition of H_2O_2 was so high that a large portion of the hydroxyl radicals were consumed by side reactions before they could be used effectively to remove Bezaktiv Brilliant Blue [37]. Therefore, we took into account the mass of 50 mg (0.33 g/L) carbon for the degradation of Bezaktiv Brilliant Blue.
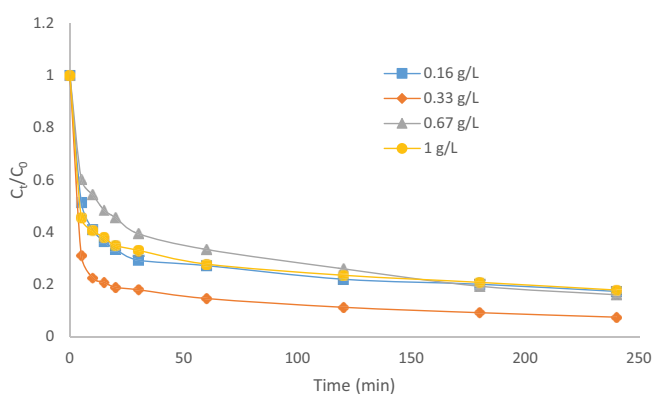
3.5.3. Influence of the initial concentration of Bezaktiv Brilliant Blue

To study the influence of dye concentration on the degradation capacity of activated carbon, Bezaktiv Brilliant Blue solutions were prepared with concentration varying from 50 to 150 mg/L, while keeping the other parameters constant. The results obtained are shown in Fig. 8.

The curves obtained in Fig. 8 show that the degradation of Bezaktiv Brilliant Blue dye on activated carbon is influenced by the initial concentration of its solution. The percentage degradation of Bezaktiv Brilliant Blue increases gradually when increasing its initial concentration. However, a decrease in the percentage of degradation is observed at initial concentrations greater than 100 ppm for the same time of 240 min. This decrease is probably due to the large number of Bezaktiv Brilliant Blue molecules present in the solution for the same number of hydroxyl radicals formed. The high initial concentration of the dye creates a competitive adsorption on the surface of the ferromagnetic activated carbon between the molecules of Bezaktiv Brilliant Blue on the one hand and the adsorption of the intermediate degradation products or by-products on the other hand. Degradation reduces the number of catalytic sites during the reaction and hence the percentage of dye removed [34]. For the removal of pollutants, it is critical to obtain a contact time that is economical and enough to remove pollutants in a conscionable condition [38].

3.5.4. Influence of H_2O_2 concentration

The degradation of Bezaktiv Brilliant Blue by the Fenton process was studied at different concentrations of H_2O_2 and the results obtained are illustrated in Fig. 9.

The curves in Fig. 9 show that increasing the concentration of hydrogen peroxide (H_2O_2) from 4 to 17 mol/L leads to a corresponding increase in the degradation from 81% to 90% at 240 min of the pollutant in solution and the dye degradation rate depends on the H_2O_2 concentration and that the presence of H_2O_2 improves the percentage of degradation. Numerous studies have proposed that the addition of oxidants, such as H_2O_2, eliminates the recombination process as the added oxidants rapidly react with conduction

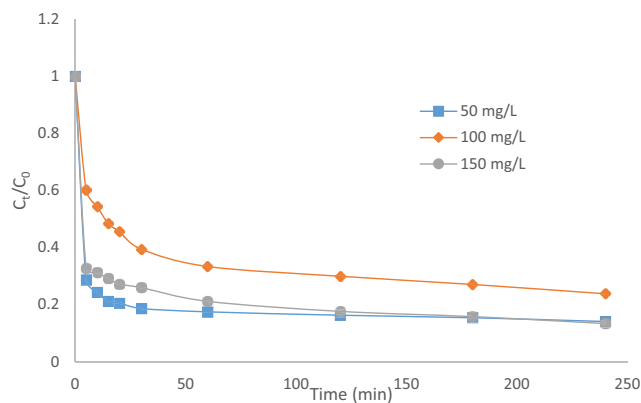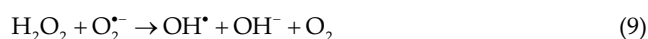Fig. 7. Influence of the mass of CA-HP@FeII on the degradation of Bezaktiv Brilliant Blue; Operating conditions: v = 150 mL, pH = 3, C_0 = 100 mg/L and [H_2O_2] = 17 mol/L

Fig. 8. Influence of Bezaktiv Brilliant Blue concentration. Operating conditions: v = 150 mL, pH = 3, m = 0.33 g/L and [H_2O_2] = 17 mol/L.

band electrons, generating extremely reactive oxidizing radicals, which increase the efficiency of Fe^{2+} as a catalyst. Consequently, an electron acceptor (H_2O_2) was used in this investigation to inhibit the recombination of electron–hole pairs and improve the photo-degradation efficiency of UV/Fe^{2+}. Other transformations of H_2O_2 generate the production of $HO^\bullet$ radicals [39]. The different mechanisms of decomposition and production of hydroxyl radicals can be described as follows [40,41]:

$$H_2O_2 + e^- \rightarrow OH^\bullet + OH^- \tag{6}$$

$$2H_2O_2 + Energy \rightarrow 2OH^\bullet \tag{7}$$

$$H_2O_2 + H^+ + e^- \rightarrow OH^\bullet + H_2O \tag{8}$$

$$H_2O_2 + O_2^{\bullet-} \rightarrow OH^\bullet + OH^- + O_2 \tag{9}$$

It appears from these equations that the addition of hydrogen peroxide leads to the additional production of $HO^\bullet$ radicals and therefore an increase in the rate of oxidation. The results obtained confirmed those existing in the literature [40,42,43]. During the process, regeneration of the ferrous ion in presence of hydrogen peroxide and hydroperoxyl radical takes place. The reactions are an advantage for the Fenton process in terms of additional degradation by ferrous ions, which allow the production of many more $HO^\bullet$ radicals that will lead to further degradation of organic molecules [44].

3.6. Kinetic approach during the Fenton process

Many processes can contribute to increase or decrease the apparent rate of the Fenton reaction, hence the complexity of extracting the kinetics of degradation of organic pollutant and H_2O_2 decomposition [45]. For the sake of simplification, the degradation reaction of an organic compound by the Fenton process has been described by a pseudo-first-order kinetic law, which considers that the concentration of hydroxyl radicals generated in the medium is quasi-stationary:
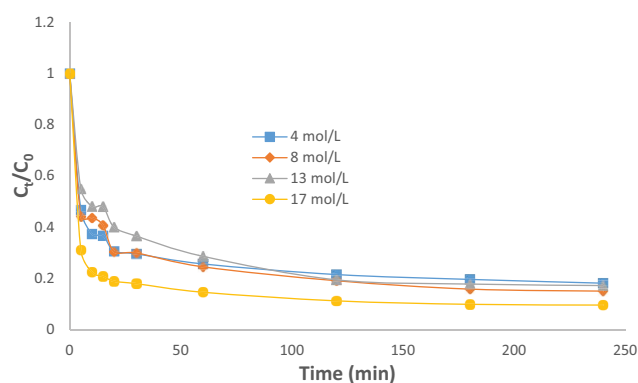

Fig. 9. Influence of H_2O_2 concentration on the degradation of Bezaktiv Brilliant Blue. Operating conditions: v = 150 mL, pH = 3, m = 50 mg and C_0 = 100 mg/L.

$$\frac{dC}{dt} = -kC \rightarrow \ln\frac{C_0}{C_t} = kt \tag{10}$$

where k the apparent rate constant, C_t and C_0 the concentrations of Bezaktiv Brilliant Blue at times t and t = 0, respectively. The second-order kinetic model was also used to describe the degradation of an organic dye by the Fenton process [46]:

$$\frac{dC}{dt} = -kC^2 \rightarrow \frac{1}{C_t} - \frac{1}{C_0} = kt \tag{11}$$

By monitoring the degradation of the pollutant as a function of time, it is possible to estimate the kinetic constant of the pseudo-first-order and pseudo-second-order using the linear regression of the experimental points. The determination of the kinetic parameters can only be carried out at the start of the reaction, when the intermediates have not yet been formed [47].

The results in Fig. 10 indicate that first-order and second-order kinetic models are appropriate to describe the degradation phenomenon. These results suggest that the chromophore degradation step followed the same mechanism in these different media, probably involving –NH– group reduction [48]. The second-order model has correlation coefficients close to unity and involves a fast kinetics right from the first minutes.

3.7. Proposal of the pollutant degradation mechanism

Fig. 10 below proposes a degradation mechanism of Bezaktiv Brilliant Blue in the presence of $^\bullet OH$ radicals.

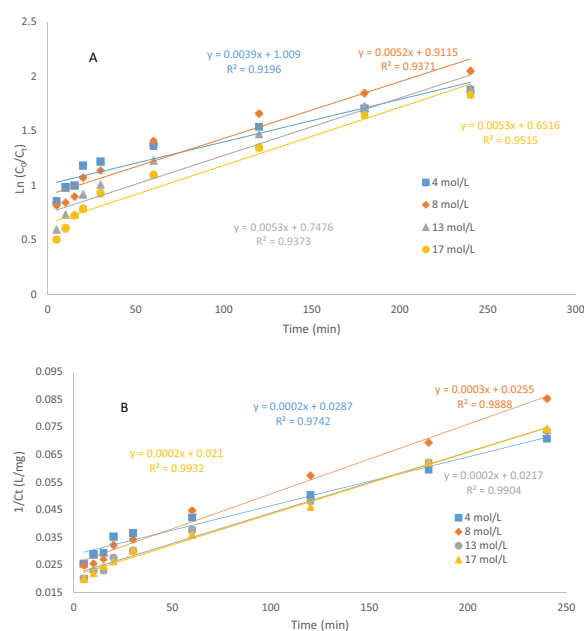From Fig. 11 it can be seen that the degradation occurs in 6 stages, namely:

Fig. 10. Pseudo-first-order (A) and pseudo-second-order (B) kinetic model of Bezaktiv Brilliant Blue degradation.
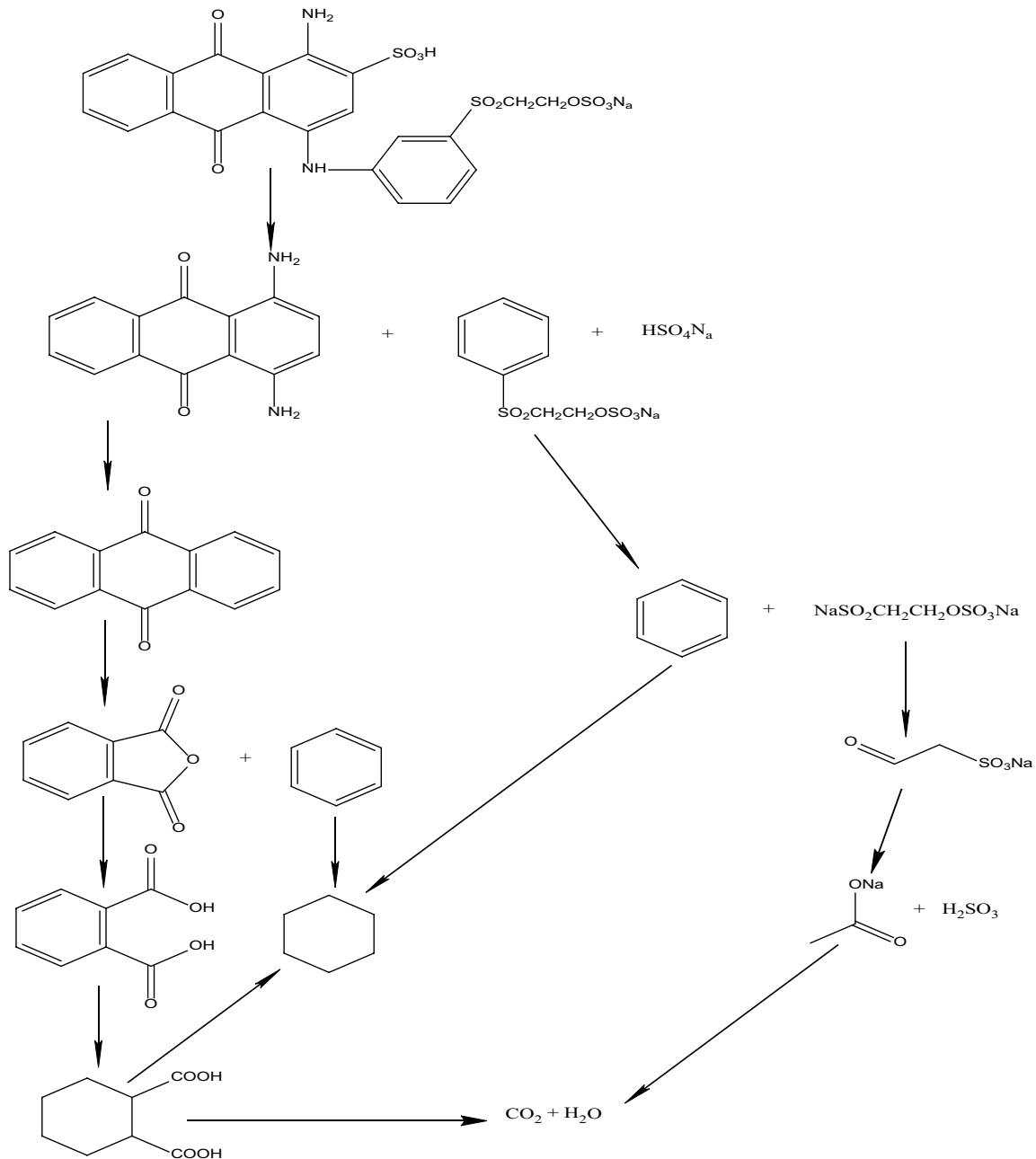
Fig. 11. Major degradation pathways for Bezaktiv Brilliant Blue dyes based on the identification of by-products.

Step 1

Desulphonation of the Bezaktiv Brilliant Blue as starting molecule which will give 2 major products among which an amino anthraquinone and a sulphonated derivative.

Step 2

The 1,4-diaminoanthraquinone obtained will lose its two amine groups which leads to 9,10-anthraquinone;

The sulfonated derivative will undergo desulfonation and will lead to a molecule of benzene, and then cyclohexane;

Step 3

The anthraquinone itself will undergo oxidation to give phthalic anhydride and a molecule of benzene.

Step 4

Hydration of the phthalic anhydride leads to a molecule of phthalic acid.

Step 5

Under certain conditions, the phthalic anhydride itself will lose its aromaticity to give 1,4-cyclohexanedicarboxylic acid.
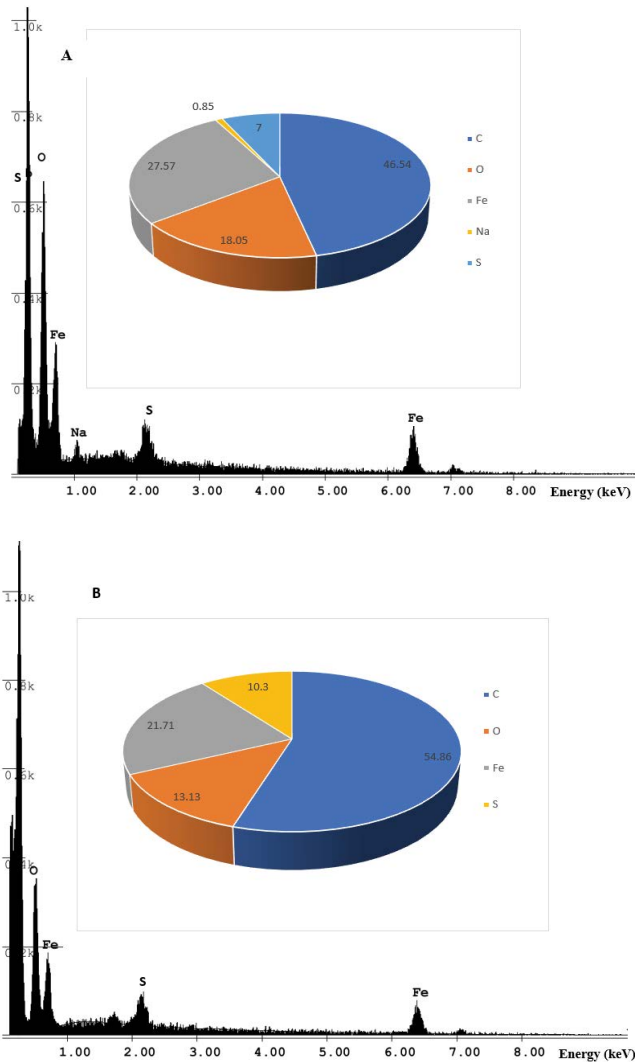
Fig. 12. Energy-dispersive X-ray spectroscopy analysis of sample CA-HP@FeII (A) and CA-HP@FeII-D (B).

Step 6

The latter can lead to 2 products: a molecule of cyclohexane or by controlled oxidation to molecules of CO_2 and H_2O.

3.8. Characterization of the material after degradation

After degradation, we tried to analyze the material again to find out if it had undergone any modification. Fig. 12 presents the result of the EDX analysis.

It can be seen from these two figures that the percentages of the elements are not identical. The change in the percentage of carbon from 46.54% to 54.86% can be attributed to the mineralization of the carbon atoms of Bezaktiv Brilliant Blue. We also observe the decrease in the percentage of iron, and this is attributed to the reaction between iron and hydrogen peroxide. The increase in the percentage of sulfur is attributed to the degradation of the pollutant from which the residual sulfur is adsorbed by the material. FTIR analysis (Fig. 13A) shows that the two materials, CA-HP@FeII and CA-HP@FeII-D have the same functional groups on their surfaces. This shows that the use of the ferromagnetic material for the treatment of water does not affect these surface functions too much although the percentage of elements is modified between 15%–32%. The same results are shown in the XRD curve (Fig. 13B). The EDX analysis also shows that the same functions are present on the material after degradation, which confirms the fact that only iron participates in the Fenton process, and not the rest of the constituents of the carbon chain of the activated carbon. The increase in the percentage of sulfur in the material after degradation proves that the degradation has indeed taken place. Another explanation of the modification of the structure is by the phenomenon of adsorption. Due to the presence of activated carbon in the reaction medium the products resulting from the degradation were adsorbed by it.
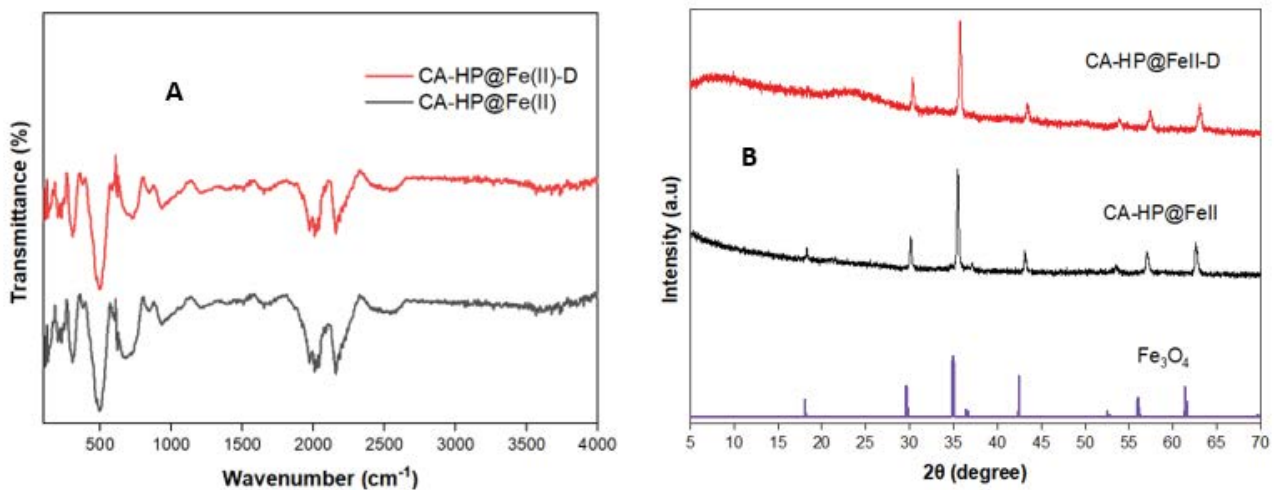

Fig. 13. Fourier-transform infrared spectroscopy (A) and X-ray diffraction (B) before and after pollutant degradation.

4. Conclusion

The preparation of activated carbon based on the hulls of rubber seeds by chemical activation with orthophosphoric acid using the response surface methodology carried out. This was followed by physico-chemical characterization of the resulting activated carbon. The factors used in the study include concentration of activating agent, the calcination temperature and the calcination time. Iodine number and yield were chosen as responses. Given the fact that the goal of this research was to prepare the most microporous activated carbon, iodine number was chosen as the result because it measures the microporosity of an activated carbon, which is the property that mainly gives the carbon its adsorbent character.

The activated carbon obtained under optimal conditions was modified by impregnation with iron sulphate heptahydrate ($FeSO_4 \cdot 7H_2O$). The ferromagnetic activated carbon obtained by modifying the activated carbon was subsequently tested for the degradation of Bezaktiv Brilliant Blue dye by the Fenton process. The study of parameters such as pH of the dye solution, concentration of H_2O_2, the initial concentration of the Bezaktiv Brilliant Blue dye and the mass of the activated carbon were highlighted, leading to a study of the kinetics of degradation process. It appears that the optimal conditions for the degradation of Bezaktiv Brilliant Blue in aqueous solution were: pH = 3; [H_2O_2] = 17 mol/L; [Bezaktiv Brilliant Blue] = 100 mg/L and the mass of activated carbon = 0.33 g/L. The general reaction mechanism for Bezaktiv Brilliant Blue mineralization by oxidative reaction occurred in the presence of $^{\bullet}OH$ radical via the Fenton oxidation process. This was possibly due to the regeneration of Fe^{2+} in the system that may have acted as a scavenging-ions to react with $^{\bullet}OH$. The characterization by FTIR spectroscopy provided information on the different characteristic functional groups on the surface of the activated carbon. The SEM/EDX analysis highlighted the presence of iron in the activated carbon, while the XRD analysis showed that activated carbon is not only amorphous but also has a crystalline structure.

Conflicts of interest

The authors declare that there are no conflicts of interest.

Acknowledgements

References

[1] D. Kouotou, H.M. Ngomo, A. Baçaoui, A. Yaacoubi, J.M. Ketcha, Physico-chemical activation of oil palm shells using response surface methodology: optimization of activated carbons preparation, Int. J. Curr. Res., 5 (2013) 431–438.

[2] T. Shalna, A. Yogamoorthi, Preparation and characterization of activated carbon from used tea dust in comparison with commercial activated carbon, Int. J. Rec. Sci. Res., 6 (2015) 2750–2755.

[3] A. Cheenmatchaya, S. Kungwankunakorn, Preparation of activated carbon derived from rice husk by simple carbonization and chemical activation for use as gasoline adsorbent, Int. J. Environ. Sci. Dev., 5 (2014) 171–176.

[4] S. Joshi, M. Adhikari, B.P. Pokharel, R.R. Pradhananga, Effects of activating agent on the activated carbon from lapsi seed stone, Res. J. Chem. Sci., 2 (2012) 80–86.

[5] R.M. Shrestha, A.P. Yadav, B.P. Pokharel, R.R. Pradhananga, Preparation and characterization of activated carbon from lapsi (*Choerospondias axillaris*) seed stone by chemical activation with phosphoric acid, Res. J. Chem. Sci., 3 (2012) 34–41.

[6] A.M.S. Ngueabouo, R.F.T. Tagne, D.R.T. Tchuifon, C.G. Fotsop, A.K. Tamo, S.G. Anagho, Strategy for optimizing the synthesis and characterization of activated carbons obtained by chemical activation of coffee husk, Mater. Adv., 3 (2022) 8361–8374.

[7] J. Bedia, M. Peñas-Garzón, A. Gómez-Avilés, J.J. Rodriguez, C. Belver, Review on activated carbons by chemical activation with $FeCl_3$, J. Carbon Res., 6 (2020) 1–25.

[8] C.S. Ngakou, H.M. Ngomo, D.R.T. Tchuifon, S.G. Anagho, Optimisation of activated carbon preparation by chemical activation of *Ayous* sawdust, *Cucurbitaceae* peelings and hen egg shells using response surface methodology, Int. Res. J. Pure Appl. Chem., 14 (2017) 1–12.

[9] A.S. Devi, M.H. Kalavathy, L.R. Miranda, Optimization of the process parameters for the preparation of activated carbon from low-cost phoenix dactylifera using response surface methodology, Austin Chem. Eng., 2 (2015) 1021.

[10] B.A. Hédi, M. Aicha, T. Nabil, Preparation of activated carbon from date stones: optimization on removal of indigo carmine from aqueous solution using a two-level full factorial design, Int. J. Eng. Res. Gen. Sci., 3 (2015) 6–17.

[11] A. Lunhong, J. Jiang, Fast removal of organic dyes from aqueous solution by AC/ferrospinel composite, Desalination, 262 (2010) 134–140.

[12] Q. Li, S. Wu, G. Liu, X. Liao, Simultaneous biosorption of cadmium(II) and lead(II) ions by pretreated biomass of *Phanerochaete chrysosporium*, Sep. Purif. Technol., 34 (2004) 925–940.

[13] B. Kakavandi, A.J. Jafari, R.R. Kalantary, S. Nasseri, A. Ameri, A. Esrafily, Synthesis and properties of Fe_3O_4-activated carbon magnetic nanoparticles for removal of aniline from aqueous solution: equilibrium, kinetic and thermodynamic studies, *Iran. J. Environ. Health Sci. Eng.*, 10 (2013) 1–9.

[14] H.S. Nadjet, Etude de la dégradation photocatalytique de polluants organiques en présence de dioxyde de titane, en suspension aqueuse et en lit fixe, Université de Grenoble, Université Mentouri (Constantine, Algérie), 2012.

[15] J. Scaria, A. Gopinath, P.V. Nidheesh, A versatile strategy to eliminate emerging contaminants from the aqueous environment: heterogeneous Fenton process, J. Cleaner Prod., 278 (2021) 1–22.

[16] P.V. Nidheesh, Heterogeneous Fenton catalysts for the abatement of organic pollutants from aqueous solution: a review, R. Soc. Chem., 5 (2015) 40552–40577.

[17] A.Y. Aydar, Utilization of Response Surface Methodology in Optimization of Extraction of Plant Materials, V. Silva, Ed., Statistical Approaches with Emphasis on Design of Experiments Applied to Chemical Processes, IntechOpen, 2018, doi: 10.5772/intechopen.73690.

[18] M.H. Do, N.H. Phan, T.D. Nguyen, T.T.S. Pham, V.K. Nguyen, T.T.T. Vu, T.K.P. Nguyen, Activated carbon/Fe_3O_4 nanoparticle composite: fabrication, methyl orange removal and regeneration by hydrogen peroxide, Chemosphere, 85 (2011) 1269–1276.

[19] D.R.T. Tchuifon, S.G. Anagho, J.M. Ketcha, G.N. Nche, J.N. Ndi, Kinetics and equilibrium studies of adsorption of phenol in aqueous solution onto activated carbon prepared from rice and coffee husks, Int. J. Eng. Technol. Res., 2 (2014) 166–173.

[20] S. Timur, I.C. Kantradli, E. Ikizoglu, J. Yanik, Preparation of activated carbons from *Oreganum* stalks by chemical activation, Energy Fuels, 20 (2006) 2636–2641.

[21] I. Tchakala, M.L. Bawa, D.G. Boundjou, K.S. Doni, P. Nambo, Optimisation du procédé de préparation des Charbons Actifs par voie chimique (H_3PO_4) à partir des tourteaux de Karité et des tourteaux de Coton, Int. J. Biol. Chem. Sci., 6 (2012.) 461–478.

[22] P.G. Udofia, P.J. Udoudo, N.O. Eyen, Sensory evaluation of wheat-cassava-soybean composite flour (WCS) bread by mixture experiment design, Afr. J. Food Sci., 7 (2013) 368–374.

[23] N. Howaniec, Temperature induced development of porous structure of bituminous coal chars at high pressure, J. Sustainable Min., 15 (2016) 120–124.

[24] T. Tay, S. Ucar, S. Karagöz, Preparation and characterization of activated carbon from waste biomass, J. Hazard. Mater., 165 (2009) 481–485.

[25] Q.Y. Zhang, W.W. Zhou, Y. Zhou, X.F. Wuang, J.F. Xu, Response surface methodology to design a selective co-enrichment broth of *Escherichia coli*, *Salmonella* spp. and *Staphylococcus aureus* for simultaneous detection by PCR, Microbiol. Res., 167 (2012) 405–412.

[26] K. Adinarayana, P. Ellaiah, Response surface optimization of the critical medium components for the production of alkaline protease by a newly isolated *Bacillus* sp., J. Pharm. Sci., 5 (2002) 272–278.

[27] R.B.N. Lekene, J.N. Ndi, A. Rauf, D. Kouotou, D.B.B. Placide, M.I. Bhanger, J.M. Ketcha, Optimization conditions of the preparation of activated carbon based egusi (*Cucumeropsis mannii* Naudin) seed shells for nitrate ions removal from wastewater, Am. J. Anal. Chem., 9 (2018) 439–463.

[28] L.M. Amola, T. Kamgaing, D.R.T. Tchuifon, C.D. Atemkeng, S.G. Anagho, Activated carbons based on shea nut shells (*Vitellaria paradoxa*): optimization of preparation by chemical means using response surface methodology and physico-chemical characterization, J. Mater. Sci. Chem. Eng., 8 (2020) 53–72.

[29] M. Ikram, M. Naeem, M. Zahoor, M.M. Hanafiah, A.A. Oyekanmi, R. Ullah, D.A. Al Farraj, M.S. Elshikh, I. Zekker, N. Gulfam, Biological degradation of the Azo Dye Basic Orange 2 by *Escherichia coli*: a sustainable and ecofriendly approach for the treatment of textile wastewater, Water, 14 (2022) 2063, doi: 10.3390/w14132063.

[30] J.C. Rios-Hurtado, E.M. Muzquiz-Ramos, A. Zugasti-Cruz, D.A. Cortes-Hernandez, Mechanosynthesis as a simple method to obtain a magnetic composite (activated carbon/Fe_3O_4) for hyperthermia treatment, J. Biomater. Nanobiotechnol., 7 (2016) 19–28.

[31] A.M. Puziy, O.I. Poddubnaya, A. Martınez-Alonso, F. Suárez-Garcıa, J.M.D. Tascón, Synthetic carbons activated with phosphoric acid: II. porous structure, Carbon, 40 (2002) 1507–1519.

[32] M. Dong, H. Zhou, W. Liu, C. He, Activated carbon prepared from semi-coke as an effective adsorbent for dyes, Pol. J. Environ. Stud., 29 (2020) 1137–1142.

[33] M. Ziati, Adsorption et électro-sorption de l'arsenic (III) sur charbon à base de noyaux de dattes activés thermiquement et chimiquement, Thèse de doctorat, Université Badji Mokhtar Annaba, Annaba-Algérie, 2012, 136 pp.

[34] G.M.R. Kpinsoton, Elaboration des catalyseurs à base de charbons actifs et de latérites pour la dégradation du bleu de méthylène par procédé fenton hétérogène, Thèse de Doctorat/Ph.D., Institut 2IE, Ouagadougou, Burkina Faso, 2019, p. 179.

[35] X.R. Xu, Z.Y. Zhao, X.Y. Li, J.D. Gu, Chemical oxidative degradation of methyl tert-butyl ether in aqueous solution by Fenton's reagent, Chemosphere, 55 (2004) 73–79.

[36] A. Stefánsson, Iron(III) hydrolysis and solubility at 25°C, Environ. Sci. Technol., 41 (2007) 6117–6123.

[37] Y.L. Song, J.T. Li, H. Chen, Degradation of C.I. Acid Red 88 aqueous solution by combination of Fenton's reagent and ultrasound irradiation, J. Chem. Technol. Biotechnol., 84 (2009) 578–583.

[38] H.S. Son, J.K. Im, K.D. Zoh, A Fenton-like degradation mechanism for 1,4-dioxane using zero-valent iron (FeO) and UV light, Water Res., 43 (2009) 1457–1463.

[39] J. Chen, M. Lui, L. Zhang, J. Zhang, L. Jin, Application of nano-TiO_2 towards polluted water treatment combined with electro-photochemical method, Water Res., 37 (2003) 3815–3820.

[40] I.K. Konstantinou, T.A. Albanis, TiO_2-assisted photocatalytic degradation of azo dyes in aqueous solution: kinetic and mechanistic investigations. A review, Appl. Catal., B, 49 (2004) 1–14.

[41] P. Saritha, C. Aparna, V. Himabindu, Y. Anjaneyulu, Comparison of various advanced oxidation processes for the degradation of 4-chloro-2-nitrophenol, J. Hazard. Mater., 149 (2007) 609–614.

[42] C.M. So, M.Y. Cheng, J.C. Yu, P.K. Wong, Degradation of azo dye Procion Red MX-5B by photocatalytic oxidation, Chemosphere, 46 (2002) 905–912.

[43] M. Saquib, M. Muneer, TiO_2-mediated photocatalytic degradation of a triphenylmethane dye (gentian violet), in aqueous suspensions, Dyes Pigm., 56 (2003) 37–49.

[44] A. Bopda, S.G.M. Mafo, J.N. Ndongmo, G.T. Kenda, C.G. Fotsop, I.-H.T. Kuete, C.S. Ngakou, D.R.T. Tchuifon, A.K. Tamo, G.N.-A. Nche, S.G. Anagho, Ferromagnetic biochar prepared from hydrothermally modified calcined mango seeds for Fenton-like degradation of Indigo Carmine, 8 (2022) 81, doi: 10.3390/c8040081.

[45] N. Um, T. Hirato, Precipitation of cerium sulfate converted from cerium oxide in sulfuric acid solutions and the conversion kinetics, Mater. Trans., 53 (2012) 1986–1991.

[46] S.A. Hayes, P. Yu, T.J. O'Keefe, M.J. O'Keefe, J.O. Stoffer, The phase stability of cerium species in aqueous systems I. E-pH diagram for the Ce-$HClO_4$-H_2O system, J. Electrochem. Soc., 149 (2002) 623–630.

[47] Y. Wang, X. Shen, F. Chen, Improving the catalytic activity of CeO_2/H_2O_2 system by sulfation pretreatment of CeO_2, J. Mol. Catal. A, 381 (2014) 38–45.

[48] S.P. Wellington, S.F. Renato, Azo dye degradation by recycled waste zero-valent iron powder, *J. Braz. Chem. Soc.*, 17 (2006) 832–838.